Agricultural and Forest Meteorology 198–199 (2014) 142–154

Contents lists available at ScienceDirect

Agricultural and Forest Meteorology

journal homepage: www.elsevier.com/locate/agrformet

Simulating impacts of water stress on woody biomass in the southern boreal region of western Canada using a dynamic vegetation model

Kuo-Hsien Chang[a,*], David T. Price[b], Jing M. Chen[a], Werner A. Kurz[c], Céline Boisvenue[c], Edward H. Hogg[b], T. Andrew Black[d], Alemu Gonsamo[a], Chaoyang Wu[a], Robbie A. Hember[e,c]

[a] Department of Geography, University of Toronto, Toronto, ON, Canada
[b] Northern Forestry Centre, Canadian Forest Service, Edmonton, AB, Canada
[c] Pacific Forestry Centre, Canadian Forest Service, Victoria, BC, Canada
[d] Agricultural Sciences, University of British Columbia, Vancouver, BC, Canada
[e] Faculty of Forestry, University of British Columbia, Vancouver, BC, Canada

ARTICLE INFO

Article history:
Received 11 January 2014
Received in revised form 17 July 2014
Accepted 24 July 2014
Available online 3 September 2014

Keywords:
Can-IBIS
Drought
Water stress
Biomass
Aspen

ABSTRACT

Drought-related dieback of aspen-dominated woodland has been a persistent and possibly increasing phenomenon over recent decades in the southern boreal forests of western Canada. The Integrated BIosphere Simulator (IBIS) dynamic vegetation model was modified for Canadian ecosystems (hence "Can-IBIS") and used to simulate effects of water stress on the woody biomass of aspen-dominated stands in the boreal mixedwood regions of Saskatchewan and Alberta. The modified model was evaluated using eddy-covariance measurements of CO_2 and water vapor fluxes made at a forested site and a grassland site located in the study region. The tested model captured 74% of the variation in biomass growth trajectories at 13 boreal and 12 parkland field study sites; the mean difference between simulated and observed values was approximately 1100 g C m^{-2}. Under the combined influences of climatic variation and increasing atmospheric CO_2 from 2000 to 2008, simulated values of net biomass growth were 544 and 240 g C m^{-2} for the boreal and parkland study sites, respectively. Drought-induced biomass losses at the drier sites (in both boreal and parkland regions) were simulated to be 100–350 g C m^{-2}, corresponding to an annual modeled mortality rate of 5–7% during severe drought years. These results were consistent with field measurements and other statistical studies. Changes in biomass over the nine-year period varied with geographical location and corresponded to spatial variation in monthly values of the self-calibrated Palmer Drought Severity Index. We conclude that Can-IBIS can be used to investigate annual impacts of water stress on woody biomass growth, although cumulative physiological effects of multi-year droughts on tree mortality would benefit from improved simulation of subgrid-scale (soil texture-driven) processes. In particular, two areas for further development are: (1) calibration based on the results of soil surveys at fine spatial/temporal scales; and (2) biophysical experiments to refine the representation of water stress constraints on biomass turnover.

1. Introduction

Recent effects of large-scale droughts on forest productivity have been widely reported (e.g., Allen et al., 2010; Schwalm et al., 2012; van der Molen et al., 2011; Zhao and Running, 2010), some of which may have the potential to alter the composition, structure, and biogeography of forests in many regions. In regions that are already subject to frequent droughts, such as the prairies and southern boreal forests of western Canada, climate warming is expected to continue, causing a reduction in ecosystem carbon sinks and possibly triggering the replacement of forest by parkland, shrubland or grassland ecosystems. The potential consequences of a warmer and generally drier climate for forest carbon stocks at continental to global scales imply an urgent need to improve understanding of the effects of drought, and of the mechanisms of water stress, on forest ecosystems.

Canada's boreal forest land area covers 309 Mha and 8% of the world's forest (Brandt et al., 2013), located in a high latitude region where climate warming is predicted to occur at approximately

* Corresponding author. Tel.: +1 5194006386.
E-mail addresses: changks888@gmail.com, kchang@alumni.uoguelph.ca (K.-H. Chang).

http://dx.doi.org/10.1016/j.agrformet.2014.07.013
0168-1923/

double the global average rate (IPCC, 2007). Climate change-induced droughts would cause increased losses of carbon to the atmosphere, through increased tree mortality, accelerated decomposition of dead organic material, reduced net ecosystem productivity (NEP), and by contributing to increased occurrence of wildfires. In Canada, the forest ecosystems most sensitive to drought are generally to be found in the southern ecoregions of the western boreal zone—which are characterized by relatively low annual precipitation and high evaporative demand during summer. Two central questions are: What is the significance of drought as a driver of large-scale tree mortality and, how can the effects of water stress on forest biomass be accounted for in dynamic vegetation models?

Recent analyses of permanent sample plot measurements (Ma et al., 2012; Peng et al., 2011) indicate that the rate of biomass change in Canadian boreal forests has varied with climatic regions. It appears that forest biomass has declined significantly in recent decades in some western Canadian boreal forests, though comparable trends were not found in eastern Canada. In reality, responses of vegetation to drought are likely to include reduced photosynthesis (Adams et al., 2009; Garcia-Quijano and Barros, 2005; Quillet et al., 2010), increased allocation to fine roots (Di Iorio et al., 2011; Wang et al., 2008), reduced water uptake and transpiration (El Maayar et al., 2009; Granier et al., 2007; Zheng and Wang, 2007), foliage loss (Landhäusser and Lieffers, 2011; Worrall et al., 2008, 2010), die-back of above-ground portions (Delbart et al., 2010; Kreyling et al., 2008), and increased mortality (Allen et al., 2010; Michaelian et al., 2010; Sala, 2009; Zeppel et al., 2011). While young forest stands (Amiro et al., 2006; Hebert et al., 2006; Spies et al., 2006) and tree seedlings (Chiatante et al., 2006; Huddle and Pallardy, 1996) may be particularly sensitive, severe drought can lead to die-back or complete mortality of mature trees that is often linked to increased susceptibility to pests and/or diseases (e.g., Michaelian et al., 2010) and depletion of non-structural carbohydrate reserves (e.g., Tague et al., 2013). Better understanding of the causes of drought and the regional responses of vegetation can contribute to more explicit representation of mortality mechanisms in dynamic vegetation models (DVM) used in global climate studies (e.g., Foley et al., 1996; Quillet et al., 2010).

From a modeling perspective, water stress is generally assumed either to operate on stomatal conductance directly, or to reduce photosynthetic capacity, causing a feedback on stomatal conductance (e.g., Kucharik et al., 2000; Delbart et al., 2010; Wang et al., 2012). Dynamic schemes for allocating photosynthate (i.e., net primary production, NPP) may also imply a growth response to water stress, by increasing the fraction of NPP allocated to roots when water stress is considered to limit water uptake. In stand-based forest productivity models drought-induced mortality can be represented as reduced probability of seedling survival. For mature trees, drought effects contributing to increased individual tree death might be captured as an increase in the intrinsic ("background") mortality rate. However, many models do not represent drought effects because there are several theories about the causes of tree mortality (Quillet et al., 2010), and how these are mediated by drought, so it is difficult to decide which is the most appropriate for general application. Developing mechanistic tree mortality algorithms for use in DVMs is challenging (Wang et al., 2012), but necessary to improve the prediction of productivity responses to climate change and hence, to improve projections of future forest carbon budgets. Therefore, assessing the impacts of water stress on forest ecosystems requires a more quantitative understanding of ecophysiological responses, including drought-induced mortality mechanisms, and their consequences at fine spatial and temporal scales.

In this study, a well-established DVM was modified to simulate effects of water stress on the biomass of aspen-dominated stands in the boreal mixed wood and aspen parkland ecoregions of Saskatchewan and Alberta. Model parameterization and validation were based on meteorological and eddy-covariance data obtained from the Fluxnet-Canada archive and a regional study of aspen (*Populus tremuloides* Michx.) productivity and survival. The main objectives of this study were: (1) to simulate the major effects of drought on woody biomass using water stress constraints in a dynamic vegetation model (i.e., Can-IBIS); and (2) to investigate the sensitivity of woody biomass to varying levels of drought intensity in the southern boreal and prairie regions of western Canada.

2. Methods

2.1. Sites and measurements

The Climate Impacts on Productivity and Health of Aspen (CIPHA) study was established in 2000, to monitor health and dieback of aspen-dominated stands across the western Canadian interior (Fig. 1; also see Hogg et al., 2005; Michaelian et al., 2010). Within CIPHA, there are 13 long-term research sites located in the southern boreal forest (denoted BOR from here on) and 12 in the subhumid ecoregion that extends between the true boreal forest and the open prairies, generally known as the aspen parkland (denoted PRK from here on), as listed in Table 1. The aspen parkland is now predominantly agricultural, as most of the prairie grassland and some of the woodlands have been converted to cropland or pasture.

The ages of the 25 CIPHA sites ranged from 50 to 89 years at the end of the study period (2000–2008), with 1940 being the mean date of stand establishment. At each CIPHA study site, three pure aspen stands were selected within a maximum distance of 30 km from one another. Two plots were established in each stand, 50–100 m apart and at least 50 m from the stand edge. Total height and stem DBH (diameter at breast height, 1.3 m) of every tree in each plot was measured in 2000, 2004 and 2008 (see Hogg et al., 2005 for methodological details). Annual tree health assessments (i.e., tree status and incidence of insects, diseases, and other damage agents) were conducted within each plot during the early part of the growing seasons (late May to July) of 2000–2008. Tree-ring analysis was conducted on all plots during 2004–2005 and in 2008. Tree-ring data and tree health assessments were used to estimate annual stand-level tree biomass using the Canadian national equations of Lambert et al. (2005).

2.2. Model description

In this study, version 2.5 of the Integrated BIosphere Simulator (IBIS) of Foley et al. (1996) was modified extensively for application to Canadian forest ecosystems, and hence named "Can-IBIS". Like IBIS, Can-IBIS is a one-dimensional representation of soil, vegetation and atmosphere interactions, allowing it to be run for individual sites and on spatial grids of various scales. The model includes the soil biogeochemistry model of Kucharik et al. (2000), which is based in turn on Verberne et al. (1990) and the CENTURY model of Parton et al. (1993). Litter is tracked separately from fine roots, foliage and woody biomass, and each of these are split into metabolic, structural and lignin (recalcitrant) pools in addition to microbial biomass and non-protected, protected and passive soil organic matter pools, each with appropriate decay coefficients. Can-IBIS also features a plant–soil nitrogen (N) cycling model (Liu et al., 2005), superimposed on the Kucharik et al. (2000) model, which tracks the transformations of nitrogen from above- and below-ground litter pools based on C:N ratios of each litter and soil C component and a set of N control modifiers. The resulting concentrations of soil nitrate and ammonium are combined with

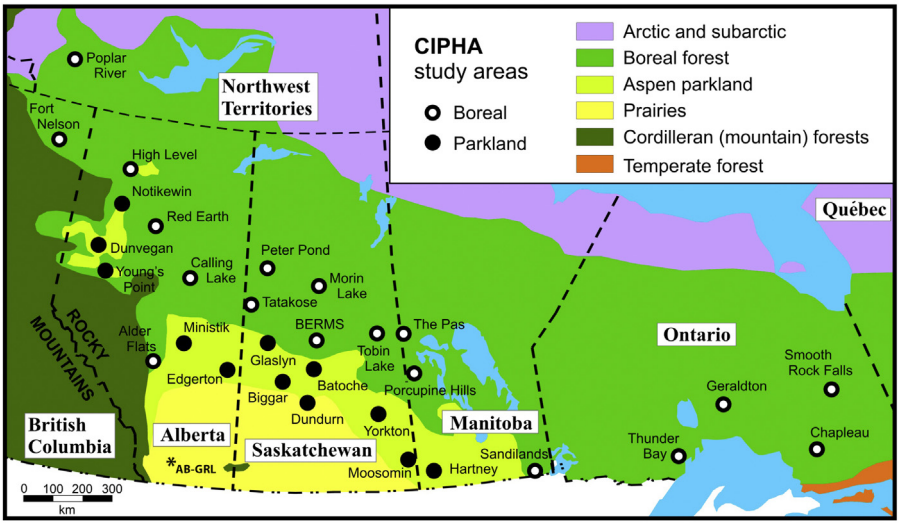

Fig. 1. Location of CIPHA study area in western Canada (also see Hogg et al., 2005; Michaelian et al., 2010). Symbols show locations of the 25 sampling sites monitored annually during 2000–2008. Open and closed circles indicate the sampling sites located in boreal (BOR) and parkland (PRK) ecoregions, respectively. The symbol * indicates the location of the Alberta grassland flux measurement site (AB-GRL). These sites were used to assess the performance of Can-IBIS with one set of parameters in simulating soil water constraints on woody biomass of trembling aspen forests in western Canada.

simulated soil water uptake rates, and provide a dynamic constraint on the photosynthetic capacities of each plant functional type (PFT).

In IBIS, vegetation at a site or within a grid cell is represented as a dynamic subset of 12 distinct PFTs determined largely by climatic constraints. In Can-IBIS, 15 PFTs have been defined, to improve the representation of forest vegetation at the scale of the North American continent. One of these additional PFTs distinguishes boreal upland ("dry") from lowland ("wet") evergreen needleleaf forests, based on assumptions about their sensitivities to soil water stress (e.g., jack pine compared to black spruce). The second addition discriminates "cool" and "warm" temperate needleleaf evergreen forests (e.g., Douglas-fir in coastal British Columbia compared to loblolly pine in the southeastern USA). The third addition is a cold-hardy moss/lichen herbaceous PFT added to the traditional cool (C3) and warm (C4) grass PFTs. IBIS and Can-IBIS are relatively unusual DVMs in that vegetation is represented as two canopy layers, with the upper canopy consisting solely of tree PFTs and the lower canopy represented by some combination of deciduous and

Table 1
Site characteristics of the 25 CIPHA study sites. Thirteen sites are located in the boreal region and 12 sites in the parkland region. The mean annual temperatures and annual precipitations for the period of measurements were obtained from National Climate Data 200 and Information Archive, Environment Canada. The symbol ** indicates the selected five sites for the investigation of the sensitivity of simulated biomass dynamics to water stress conditions. Stand ages are reported for year 2000.

Site I.D.	Full name	Prov.	Location (°N, °W)	Elev. (m)	Age (yrs)	T_a (°C)	PPT (mm y^{-1})
Boreal region (BOR)							
ALD	Alder Flat	AB	52.7, 114.9	1058	55	4.2	539
CAL	Calling Lake	AB	55.3, 113.0	629	48	3.0	478
FIS**	Fish Lake	SK	53.6, 106.2	553	81	1.8	428
FTN	Fort Nelson	BC	58.8, 121.6	527	49	−0.2	446
HIG	High Level	AB	58.3, 117.2	346	58	0.9	373
MOR	Morin Lake	SK	55.2, 106.1	434	63	0.3	531
PAS	The Pas	MB	53.6, 101.7	288	57	1.8	308
PET	Peter Pond	SK	55.7, 108.8	471	52	1.3	487
POP	Poplar River	NT	61.3, 121.7	244	57	−2.6	408
POR	Porcupine Hills	MB	52.5, 101.2	661	79	2.0	336
RED	Red Earth	AB	56.6, 115.3	514	48	1.6	370
TAT	Tatakose	SK	54.6, 109.9	665	58	1.5	427
TOB	Tobin Lake	SK	53.8, 103.0	300	57	1.2	470
			Average	**515**	**59**	**1.5**	**431**
Parkland region (PRK)							
BAT	Batoche	SK	52.7, 106.1	504	79.0	3.5	359
BIG	Biggar	SK	52.4, 107.8	746	52.0	2.8	412
DUN**	Dundurn	SK	51.7, 106.7	542	61.2	3.8	353
DVG	Dunvegan	AB	55.8, 118.2	569	56.0	2.8	419
EDG**	Edgerton	AB	52.6, 110.6	696	66.2	3.7	382
GLA	Glaslyn	SK	53.6, 108.6	688	75.2	1.2	456
HAR	Hartney	MB	49.5, 100.8	448	59.7	3.7	508
MIN	Ministik	AB	53.3, 112.9	771	71.5	2.5	387
MOO	Moosomin	SK	49.8, 101.8	592	45.5	4.2	443
NOT**	Notikewan	AB	57.3, 117.2	457	66.3	3.1	336
YPT	Youngs Point	AB	55.2, 117.6	748	55.0	3.2	543
YRK**	Yorkton	SK	51.3, 103.1	654	52.7	1.8	507
			Average	**618**	**61.7**	**3.0**	**425**

evergreen shrub PFTs along with one or possibly two herbaceous PFTs.

The canopy and soil hydrology modules are based on the LSX land surface transfer scheme (Bonan, 1994; Thompson and Pollard, 1995a,b) and are used to calculate canopy energy fluxes, as well as a one-dimensional water balance, which accounts for interception of rain and snowfall, soil moisture flows, root water uptake, infiltration, runoff and drainage from the base of the soil profile. Standard soil textural classes are applied to each soil layer to compute temperature, water and ice content in the soil column in each grid cell. Six to eight soil layers, with nominal thicknesses of 0.1, 0.15, 0.25, 0.5, 1.0, 2.0, 4.0, and 4.0 m, respectively (for a total depth of 4 to 12 m) can be used, depending on application. Usually the top four layers are considered rootable (with a combined depth of 1 m or less) overlaying two to four deeper and thicker layers needed to simulate vertical flows of heat and water in a somewhat realistic manner. Snow cover accumulation is simulated in three layers above the soil surface, which affects surface albedo as well as heat exchanges between the soil and the atmosphere.

The carbon assimilation scheme in Can-IBIS is a canopy model extended to treat sunlit and shaded canopy fractions separately (unlike IBIS 2.5) with a more modular source code. Leaf-level photosynthesis follows Farquhar's model (e.g., Farquhar et al., 1980; also see El Maayar et al., 2002) and the Ball-Berry leaf conductance model (Ball et al., 1987). The model first simulates a reduction in photosynthetic capacity and decreased stomatal conductance. The notional maximum rate of photosynthesis is prescribed by a PFT-specific value for the activity of ribulose biphosphate carboxylase (Rubisco), denoted V_{cmax}, which is then modified by multipliers representing the effects of temperature, available N, and soil moisture stress. In Can-IBIS, the effect of soil water stress is represented as the minimum of two opposing functional constraints, representing the effects of soil moisture deficits (S_{dry}) and soil waterlogging (S_{wet}), where the optimum moisture content is considered to be field capacity. In the model, these PFT-specific constraints are computed for each soil layer in the rootable profile and a mean value weighted by the fraction of fine-root biomass occupying each layer is applied to the corresponding V_{cmax} as a control on the instantaneous (hourly) photosynthesis rate for that PFT. A further control on annual biomass accumulation was introduced into Can-IBIS to represent the mortality effects of seasonal water deficits and waterlogging ("flooding") events (as physiological causes of plant mortality are not explicitly recognized in standard IBIS). These functions are described in the following section.

2.2.1. Creating temporally and spatially explicit soil water stress constraints

The soil water stress constraints in Can-IBIS are determined from the fraction of total fine-root biomass (f_{root}) in the rootable layers, and the relative available soil water for plants (W_{root}) given by

$$W_{root} = \frac{W_{soil} - S_{wilt}}{S_{field} - S_{wilt}} \quad (1)$$

where W_{soil} is the volumetric soil water content, and S_{wilt}, and S_{field} are the volumetric soil water contents at wilting point and field capacity, respectively. The convention adopted in Can-IBIS (as in IBIS) is that any water present in the soil as ice reduces the porosity, and allows the remaining liquid water content to be expressed as a fraction of the remaining pore space. The vertical root profile was distributed throughout the rootable soil layers to account for the capability of root water uptake using:

$$\sum_{rlayer=1}^{rlayer=4} f_{root} = \sum_{rlayer=1}^{rlayer=4} (1 - \beta^{H_{rlayer}}) = 1 \quad (2)$$

where f_{root} in the rootable soil layers sums to 1, and H_{rlayer} is the thickness of each layer. In the simulations reported here, seven soil layers (total profile depth of 8 m) were used, with the top four soil layers (i.e., 0.1, 0.15, 0.25, and 0.5 m) considered rootable (rlayer). The scaling coefficient β is a PFT-specific parameter (Jackson et al., 1996, 1997), to shape the profile of fine-root biomass distribution for each PFT vertically within the rootable layers. β was set to 0.95 for the boreal deciduous broadleaf PFT. Values of S_{dry} and S_{wet} were calculated at each time step based on the layer W_{soil} and f_{root}:

$$\begin{cases} S_{dry} = f_{root}\,(1 - \exp(\alpha p_{stress} W_{root})) \\ S_{wet} = f_{root}\left(1 - (\gamma p_{stress}\,(W_{soil} - S_{field}))^2\right) \end{cases} \quad (3)$$

where α was set to -1.0, representing the "intensity" of soil moisture stress effects on all plant physiological processes. We investigated the sensitivity of the model to different values for α because the default value of -5.0 has no apparent effect, and only higher (less negative) values impose greater stress levels. γ was set to 1.0 to create an inverse parabolic response of plants to water stress imposed by W_{soil} exceeding field capacity up to complete saturation. p_{stress} indicates the level of sensitivity to water stress for each PFT.

2.2.2. Applying soil water stress constraints to carbon assimilation, allocation and biomass turnover in Can-IBIS

In Can-IBIS, available water content in the root zone soil layers (W_{root}, Eq. (1)) is considered to constrain V_{cmax} for both wet and dry conditions. The dynamic allocation scheme allocates NPP to leaves and fine-roots first, based on modeled leaf area index, while maintaining these two biomass pools in a PFT-specific ratio. After these demands are met, residual NPP is allocated to woody biomass, hence carbon allocation to the stem is constrained by water stress. Furthermore, the surviving tree biomass (above- and below-ground biomass) is constrained by a dynamic function of water stress as formulated in Eqs. (4) and (5), and illustrated in Fig. 2. Values of S_{dry} and S_{wet} are expressed as alternative constraints on hourly V_{cmax} imposed by normalized W_{root} (Fig. 2(a)). Fig. 2(b) presents the exponential relationship between S_{dry} and $S_{bio,surviving}$, showing that drought-induced mortality increases with decreasing δ. The accumulation of daily soil water deficit values (given by S_{dry}) during the year is used to estimate the contribution of water deficit stress to annual biomass mortality. In this study, the cumulative impact of drought during the growing season on biomass mortality was limited to the period when W_{ice} in the top soil layer is zero. Herein, $\bar{S}_{dry,annual}$ is computed from hourly values of S_{dry} at each timestep during the growing season (defined as the period when the top soil layer is unfrozen), and applied to the biomass at the end of each year. The annual effect of drought on biomass turnover of each tree PFT ($S_{bio,surviving}$) is then expressed as an exponential function of $\bar{S}_{dry,annual}$

$$\begin{cases} \bar{S}_{dry,annual} = \left(\dfrac{\sum_{rlayer=1}^{rlayer=4} S_{dry}}{\sum dry \;\; event}\right), \quad \text{if} \quad W_{ice,rlayer=1} = 0 \\ S_{bio,surviving} = 1 - \dfrac{1}{\exp(\delta \bar{S}_{dry,annual})} \end{cases} \quad (4)$$

where $W_{ice,rlayer}$ is the volumetric ice content in the top root layer, and δ is a scaling factor to regulate the intensity of $S_{bio,surviving}$ for each PFT (set to 5.0 for the boreal tree PFTs considered here). The value of $S_{bio,surviving}$ is then applied to the biomass pools (above- and below-ground) as calculated from annual NPP.

$$C_{bio,surviving} = C_{bio} S_{bio,surviving} \quad (5)$$

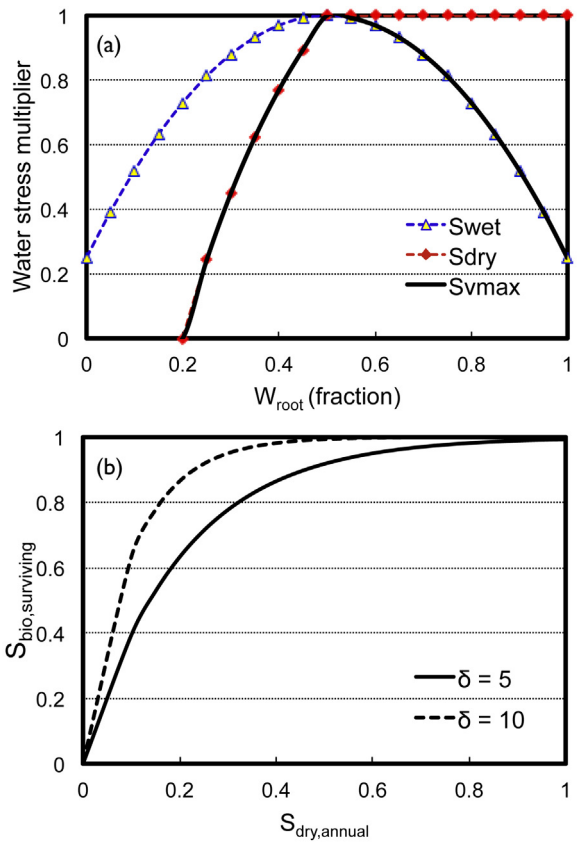

Fig. 2. Water stress response curves for the boreal deciduous broadleaf forests in Can-IBIS. (a) Responses of S_{dry} and S_{wet} (daily values of soil water stress factors) to the relative available soil water for plants (fraction, W_{root}) as multipliers ranging from 0 to 1. Values of S_{wet} and S_{dry} are used to determine a multiplier S_{vmax} for each soil layer and time step. (b) The response of biomass mortality, as determined from $S_{bio,surviving}$, to $S_{dry,annual}$ for δ at values of 5 and 10, respectively (see Eq. (4)). S_{dry} and S_{wet} are expressed as alternative constraints on V_{cmax} imposed by normalized W_{root}. Drought-induced mortality increases with decreasing δ based on the exponential relationship between S_{dry} and $S_{bio,surviving}$.

where C_{bio} is the biomass at year-end before accounting for drought-induced mortality, and $C_{bio,surviving}$ is the surviving biomass.

2.3. Can-IBIS configuration and evaluation

The spatial version of Can-IBIS was assessed by simulating biomass trends at the 25 CIPHA study sites. The model inputs included a set of gridded soils and monthly climate data (10 km × 10 km spatial resolution) covering the region of the 25 CIPHA study sites. Soil texture classes were derived from the Canadian Soil Information System (Can-SIS) Soil Landscapes of Canada (SLC) database (Soil Landscapes of Canada Working Group, 2004). Data for most climate variables (including relative humidity, solar radiation, wind speed and wet days per month) were interpolated using ANUSPLIN (e.g., Hutchinson, 2004; McKenney et al., 2006) from Meteorological Service of Canada 1961–1990 station normals, but monthly mean daily air temperature (T_a), diurnal air temperature range, and total precipitation (PPT), were interpolated from historical records for the period 1901–2010 (McKenney et al., 2011). In this study, the simulations were initialized with a 400-year spin-up to equilibrate soil organic carbon content, using detrended data referenced to the mean for 1901–1915. This was followed by the 110-year (1901–2010) historical climate run. Can-IBIS source code and climate datasets can be requested from David T Price at Canadian forest Service.

Both IBIS and Can-IBIS incorporate a version of the WGEN weather generator (Richardson and Wright, 1984) to generate daily and hourly values of weather variables from monthly input data, which are used in turn to force the model's canopy-level physical and physiological processes. A recently discovered error in the algorithm used in IBIS caused the simulated total PPT to diverge from the input value and was corrected (J.-S. Landry, personal communication, 2012). The weather generator outputs for daily and monthly 10 km grid-cell mean T_a and total PPT were compared to daily and monthly means and totals measured at two eddy-covariance flux measurement towers in the Fluxnet-Canada network, close to the simulated domain. These were the Southern Old Aspen site, located in Prince Albert National Park, Saskatchewan (Barr et al., 2007) referred to here as BOR-FIS (also a site in the CIPHA network), with a 14-year weather record, and the Alberta grassland site, located near Lethbridge, Alberta (Flanagan and Johnson, 2005), referred to here as AB-GRL with a 7-year weather record (Fig. 1).

The model's performance at reproducing soil physical and ecophysiological observations was assessed by comparing simulated data with measurements reported for soil volumetric water content (W_{soil}), W_{root}, stand latent heat flux (LE) and gross primary productivity (GPP) obtained from the Fluxnet-Canada archive. Linear regressions between observed and simulated hourly and daily means were used to calculate the coefficients of determination (R^2), intercept (INT), slope (S), and root mean square error (RMSE), which were then used as relative indices of model performance.

Five sites (namely FIS in the boreal region, and NOT, EDG, YRK and DUN in the parkland) were selected to represent the range of conditions occurring across the domain of the CIPHA study. These sites allowed a more detailed investigation of the temporal and spatial responses of biomass variations to drought from 2000 to 2008. The self-calibrated Palmer Drought Severity Index ($PDSI_{sc}$, Wells et al., 2004) was calculated using the interpolated monthly T_a and PPT time-series data for each of the 10 km grid-cells containing these five sites, using soil water-holding capacity obtained from the SLC dataset. The purpose was to provide independent indices of variations in local drought stress to compare with the variations in tree biomass both observed over the period 2000–2008 and as simulated by Can-IBIS.

Since the profile of soil texture is a critical factor influencing simulated drought stress, eight experimental soil texture profiles were compared to examine the sensitivity of W_{soil} and $S_{bio,surviving}$ to soil texture. In this experiment, the soil texture parameters were varied while all other model parameters were held constant. Table 2 lists the experimental design of eight soil texture profiles, composed of differing combinations of sand, silty loam, sandy clay, loam and clay. Based on the SLC dataset, Can-IBIS originally interpreted the soil texture profile at FIS as a loam for layers 1 to 6 (0–4 m depth) and clay for layer 7 (4–8 m depth), respectively (see Table 2, Experiment 2). In this study, we modified the soil texture based on site measurements reported by Cuenca et al. (1997) at FIS, (Table 2, Experiment 1 (the base scenario)), parameterizing silty loam and sandy clay for the upper (0–0.5 m) and deeper (>0.5 m) soil layers, respectively. Experiments 3 and 4 were parameterized to test the impacts of sand and clay soil types for the upper layers (0–0.5 m). In order to examine water holding capacity and water movement from the top to the bottom of the soil profile, Experiments 5 and 6 were parameterized with either sand or clay for the upper and deeper soil layers, respectively. Uniform soil texture profiles of either sand or clay were tested in Experiments 7 and 8 as references. These sensitivity experiments were run at BOR-FIS from 1900 to 2010 to understand the overall effects of sandy/clay soil texture profiles on relationships among annual precipitation, soil water content and drought stress.

Table 2
Eight experimental profiles of soil properties in seven soil layers for testing the model sensitivity of W_{soil} and $S_{bio,surviving}$ to soil texture. Experiment 1 (3SL + 4SC) is sandy loam and sandy clay for the top three and the bottom four soil layers, respectively, based on the study of Cuenca et al. (1997). Experiment 2 (6L + 1C) is the original model interpretation based on the SLC database, showing loam and clay for the top six and the bottom soil layers, respectively. Experiments 3 (3S + 4SC) and 4 (3C + 4SC) are sandy clay in the bottom four soil layers combined with sand and clay for top three soil layers, respectively. Experiments 5 (6S + 1C) and 6 (6C + 1S) are the contracting soil profiles, combining sand and clay for the top three and the bottom four soil layers. Experiments 7 and 8 are the uniform soil profile of sand and clay, respectively.

Experiment	Code	Soil texture profile	Clay:sand:silt (%)	Porosity (%)	Field capacity ($m^3\ m^{-3}$)
1	3SL + 4SC	Layers 1–3 (0–0.5 m): sandy loam	15:20:65	50.1	0.330
		Layers 4–7 (0.5–8 m): sandy clay	40:53:7	43.0	0.339
2	6L + 1C	Layers 1–6 (0–4 m): loam	18:42:40	46.3	0.270
		Layer 7 (4–8 m): clay	60:20:20	47.5	0.396
3	3S + 4SC	Layers 1–3 (0–0.5 m): sand	3:92:5	43.7	0.091
		Layers 4–7 (0.5–8 m): sandy clay	40:53:7		
4	3C + 4SC	Layers 1–3 (0–0.5 m): clay	60:20:20	47.5	0.396
		Layers 4–7 (0.5–8 m): sandy clay	40:53:7	43.0	0.339
5	6S + 1C	Layers 1–6 (0–4 m): sand	3:92:5	43.7	0.091
		Layer 7 (4–8 m): clay	60:20:20	47.5	0.396
6	6C + 1S	Layers 1–6 (0–4 m): clay	60:20:20	47.5	0.396
		Layer 7 (4–8 m): sand	3:92:5	43.7	0.091
7	7S	Layers 1–7 (0–8 m): sand	3:92:5	43.7	0.091
8	7C	Layers 1–7 (0–8 m): clay	60:20:20	47.5	0.396

3. Results

3.1. Can-IBIS evaluation

3.1.1. Woody biomass responses to climatic constraints and soil water deficits

Fig. 3 shows that f_{root} dynamics corresponded to seasonal and interannual variations in rainfall and snowfall, indicating relatively low W_{root} in the dry years 2001–2002, followed by generally greater soil water content from 2004 onwards. Fig. 3(c) shows the approximate covariance of annual water stress and simulated woody biomass during 2000–2008. $S_{bio,surviving}$ was noticeably lower during the summers of 2001–2002.

3.1.2. Importance of interannual climate variability for simulating drought-related mortality

Hourly measurements of T_a and PPT obtained at BOR-FIS and AB-GRL were used to assess the reliability of the IBIS implementation of WGEN at daily and monthly time steps (See Figs. S1 and S2 in Supplementary information). Simulated daily T_a agreed reasonably well with the measured data at both flux tower sites ($R^2 > 0.57$, RMSE = 6.8), whereas the amounts falling in simulated precipitation events were captured rather poorly ($R^2 > 0.25$, RMSE = 22.8). Monthly mean T_a ($R^2 > 0.91$, RMSE = 2.55) and total PPT ($R^2 > 0.49$, RMSE = 11.3) were captured more successfully. Monthly gridded climate data provide no information about the timing and intensity of the specific precipitation events that contribute to monthly totals—a limitation imposed by the practical constraints of running a climate-sensitive model at continental scales. That said, WGEN appeared to perform fairly well within the region of the CIPHA sites. Daily- and hourly-simulated meteorology were then used to simulate the climatic drivers for forest vegetation productivity and mortality in the study region.

3.1.3. Testing Can-IBIS in simulations of latent heat fluxes, soil water content, and carbon dynamics in Aspen forests

Fig. 4(a) shows that Can-IBIS was reasonably successful in simulating the range of observed W_{soil} (0.2 to 0.5 $m^3\ m^{-3}$, averaged over the top 1 m of the profile) at BOR-FIS from 1997 to 2010. Can-IBIS appears to overestimate both the rates of drainage and runoff at high W_{soil} (given that evapotranspiration is captured fairly well (Fig. 4(c)) as well as the rates of recharge during and following months with high precipitation amounts. Can-IBIS simulated higher W_{soil} during the relatively wet years after 2004. There could be significant problems with the parameterizations of soil hydrological factors such as saturated hydraulic conductivity, caused by use of gridcell mean values in the original SLC dataset in place of the measured site-level parameters. Notably, the fraction of organic matter in the surface layer could be substantially different. For the simulated 8 m soil profile (Fig. 4(b)), there was general agreement between the simulated periods of low W_{soil} (relative to the 1997–2010 mean) and the periods of low W_{soil} observed in the top 1 m (i.e., the simulated rooting depth), although the period of low moisture content began too early (2000) and finished too late (2004). This suggests a significant problem with the simulated soil hydrology, which could result from poor parameterization and/or from the assumption of an 8 m profile depth. Simulated seasonal and interannual variations in monthly LE were well correlated with observations ($R^2 = 0.66$) and also corresponded to the variations in W_{soil}. Can-IBIS was able to simulate the major variations in soil moisture content at the BOR-FIS flux tower site (Fig. 4(c)).

On the other hand, Can-IBIS captured the seasonal variations in reported GPP for the BOR-FIS site remarkably well ($R^2 = 0.92$, Fig. 4(d)). Low GPP was observed in 2001–2003 and gradually increased after this period due mainly to higher annual precipitation totals after 2003 (see Fig. S1 in SI). Another period of lower than normal precipitation occurred during 2008–2009, causing both observed and simulated GPP to decline ($\sim$1200 g C $m^{-2}\ y^{-1}$) compared to 2004–2007 (when GPP averaged 1320 g C $m^{-2}\ y^{-1}$); this decrease was presumably related to increased drought stress in 2008–2009. Hence, Can-IBIS appears able to capture large scale effects of variations in the annual water budget on GPP as estimated using eddy covariance measurements, in spite of its limitations in simulating monthly and seasonal hydrology.

3.2. Biomass simulations at 25 CIPHA sites using tested Can-IBIS

Fig. 5 shows biomass simulated by Can-IBIS as a function of stand age, compared to observations at the 25 CIPHA sites, categorized into the BOR and PRK ecoregions. Both observed and simulated data show a generally increasing biomass trend at the BOR sites, although the model significantly underestimated the measured biomass by as much as 2500 g C m^{-2} at five sites, namely BOR-PAS, BOR-PET, BOR-RED, BOR-TAT and BOR-TOB.

Both observed and simulated biomass showed relatively little change at the PRK sites. Can-IBIS was generally more accurate in simulating the observed woody biomass at these sites than at the BOR sites, but overestimated significantly at PRK-BAT and PRK-HAR. Observations showed exceptionally high, drought-induced mortality in one of the three stands at the PRK-BAT site, and two of the stands at the PRK-HAR site were destroyed by a tornado in 2007.

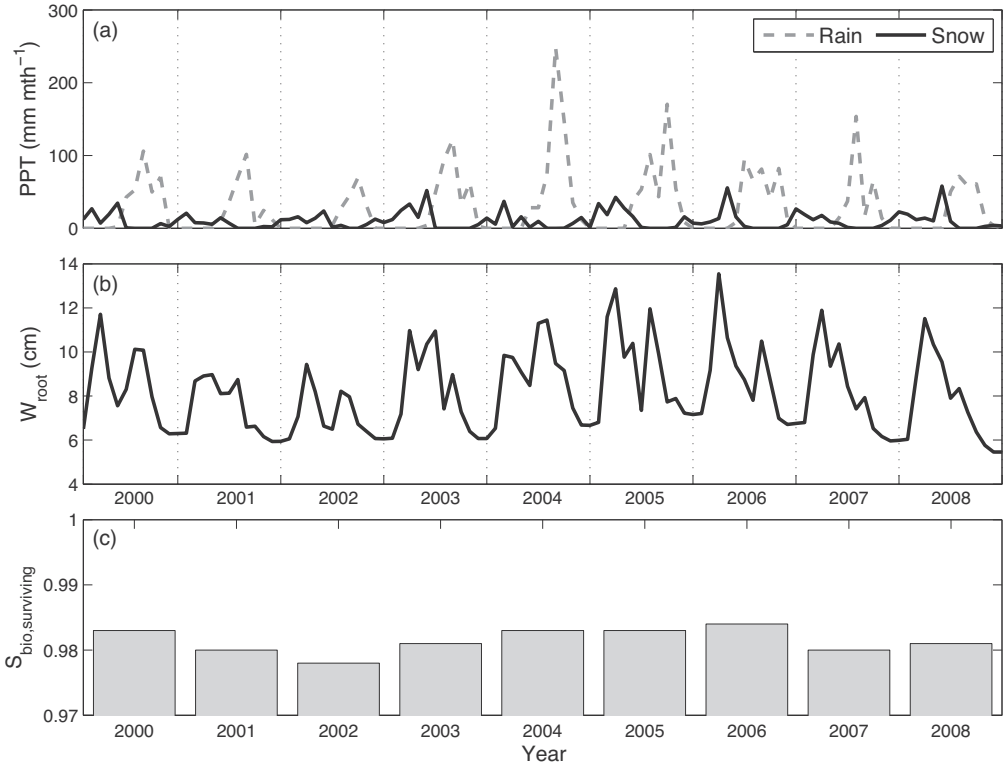

Fig. 3. Simulated variations in water stress related variables from 2000 to 2008 at PRK-EDG: (a) precipitation (i.e., monthly accumulated rain and snow); (b) relative available soil water (W_{root}, Eq. (1)) in rooting depth (i.e., $W_{root} \times H_{rlayer}$); (c) drought surviving woody biomass index ($S_{bio,surviving}$, Eq. (4)), respectively. W_{root} corresponds to seasonal and interannual variations in rainfall and snowfall; $S_{bio,surviving}$ is noticeably lower during the summers of 2001–2002. The graphs demonstrate how the Can-IBIS model captures effects of growing season water stress on mortality of woody biomass.

Overall, the model suggested that net biomass increased during the nine years from 2000 to 2008 by approximately 544 and 240 g C m^{-2} for BOR and PRK, respectively, compared with 638 and 251 g C m^{-2} obtained from measurements, respectively, over the same period. Can-IBIS was able to explain about 74% of the variation in observed biomass for all years, with R^2 of 64% and 79% for BOR and PRK, respectively (Fig. 6). The biases of simulated biomass were mainly caused by two clusters of data populations: Cluster no. 1: BOR-TOB; Cluster no. 2: BOR-PET, BOR-TAT, BOR-RED, and BOR-PAS. Across all sites over all years, Can-IBIS predicted average biomass of 7128 and 6052 g C m^{-2} for BOR and PRK, respectively, in fairly close agreement with the observations of 7628 and 5694 g C m^{-2}, respectively. In relative terms, Can-IBIS overestimated observed biomass by about 6.3% at the parkland sites and underestimated by about 7% at the boreal forest site, with an overall underestimation across all 25 CIPHA sites of approximately 1.3%.

3.3. Biomass mortality responses to drought intensity

Fig. 7(a) shows the $PDSI_{sc}$ distribution (i.e., the frequency of occurrence of monthly $PDSI_{sc}$ values grouped into integer classes) from 2000 to 2008 at the five selected sites across the CIPHA study area. The most negative $PDSI_{sc}$ (most severe drought) occurred at the BOR-FIS, PRK-EDG and PRK-NOT sites. These sites were much drier than PRK-DUN and PRK-YRK where the majority of months returned $PDSI_{sc}$ greater than 0. When comparing $PDSI_{sc}$ distribution with the observed and simulated changes in total biomass (Fig. 7(b)), the overall variation in biomass corresponded to the drought signals inferred from the regional $PDSI_{sc}$. Increases in biomass were consistent with a predominantly positive distribution of accumulated months of $PDSI_{sc}$ (sites located toward the east of the CIPHA study region), with the largest biomass growth observed and simulated at PRK-YRK. In order to examine the responses of biomass to water stress, we compared the variations in rainfall, $PDSI_{sc}$ and surviving biomass for the period 2000–2010 at BOR-FIS and PRK-EDG (Fig. 8). The shaded areas of $PDSI_{sc}$ in Fig. 8 indicate that drought was more intense in 2002–2004 and 2008–2009. At both sites, these two drought periods corresponded to annual precipitation (mainly summer rainfall) 30–50% lower than that observed in 2005.

Can-IBIS simulated increased biomass mortality in response to the more intense droughts indicated by the shaded areas of $PDSI_{sc}$ in 2001–2003 and 2008–2009 (Fig. 8(e)–(f)). However, the effect on biomass growth differed markedly between BOR-FIS and PRK-EDG, with a relatively smooth trend simulated at BOR-FIS during 2001–2003, compared to a marked decrease of ~200 g C m^{-2} y^{-1} at PRK-EDG during 2002. Although changes in observed and simulated biomass followed similar patterns at both sites, the model clearly underestimated biomass growth during the wet years of 2006–2007 at BOR-FIS. Given the apparently good estimation of GPP seen in Fig. 4(d), this could be due either to underestimation of allocation to woody biomass, or overestimation of the mortality effect at this site.

3.4. Sensitivity of soil water stress to soil texture profiles

A series of experimental simulations were conducted to examine the sensitivity of the soil model in Can-IBIS to the parameterization of soil texture, and hence to assess the realism of simulated variations on soil water content and their effects on simulated biomass. Can-IBIS simulated a plausible relationship of hydrological condition to soil texture, with lower W_{soil} simulated in sandy soil profiles and higher W_{soil} simulated in clay-dominated soil profiles (Fig. 9(a)).

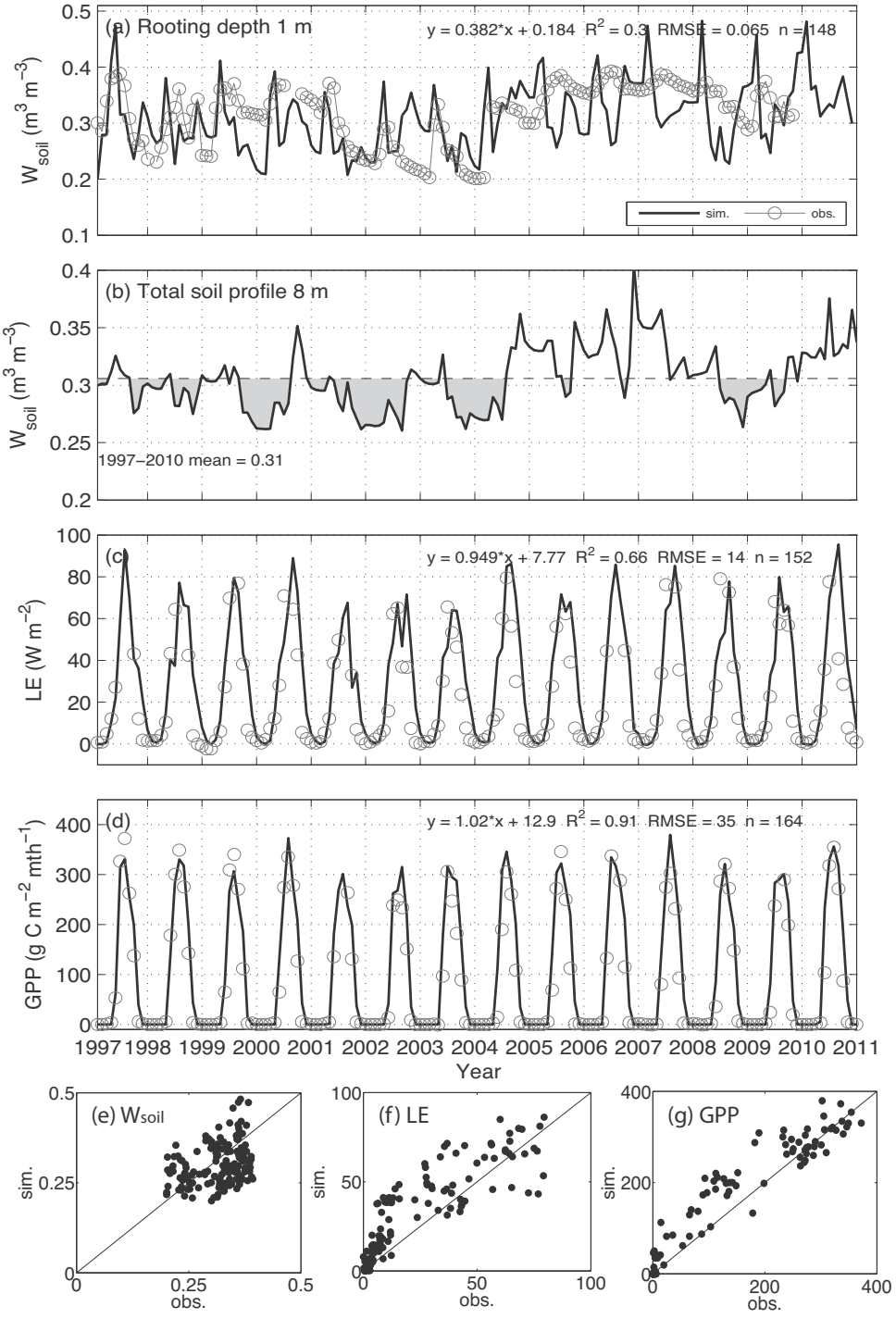

Fig. 4. Comparisons of monthly observed and simulated water and carbon cycles at BOR-FIS: (a) and (b) volumetric water content for the top 1 m (four rootable layers) and 8 m (total simulated soil depth), respectively; in (b) the shaded area indicates the period when W_{soil} was lower than the mean for the entire 1997–2010 period; (c) latent heat flux; (d) gross primary productivity. Corresponding 1:1 relationships between observed and simulated for graphs (a), (c), and (d) are shown in (e), (f) and (g). Can-IBIS appears able to capture the variations in hydrological and carbon dynamics between the transitions of dry and wet periods.

Experiments 7S and 6S + 1C shows that a bottom soil layer of clay (i.e., Layer 7, 4–8 m depth) regulated the vertical movement and storage of water throughout the profile. The results show that any soil with a bottom layer of clay will then have higher moisture content throughout the profile than any soil with a non-clay bottom layer. Furthermore, W_{soil} in rootable soil layers with a sandy texture will remain high if a clay layer is present deeper in the soil profile. Higher W_{soil} was also simulated in Experiments 3SL + 4SC, 6L + 1C, and 3C + 4SC, compared with Experiment 7S. The original input of soil texture from the 10 × 10 km gridded data set was 6L + 1C, but the data obtained from site measurements at BOR-FIS correspond more closely to 3SL + 4SC, resulting in a marginally higher W_{soil}. Comparing experiments 3SL + 4SC, 3S + 4SC and 3C + 4SC, shows that in low precipitation regimes, water storage in the soil column increases with the amount of clay in the top 0.5 m soil depth.

Fig. 9(b) shows the dependence of the $S_{bio,surviving}$ multiplier on the different soil texture profiles. Higher $S_{bio,surviving}$ generally occurred under higher W_{soil} as a result of higher soil water

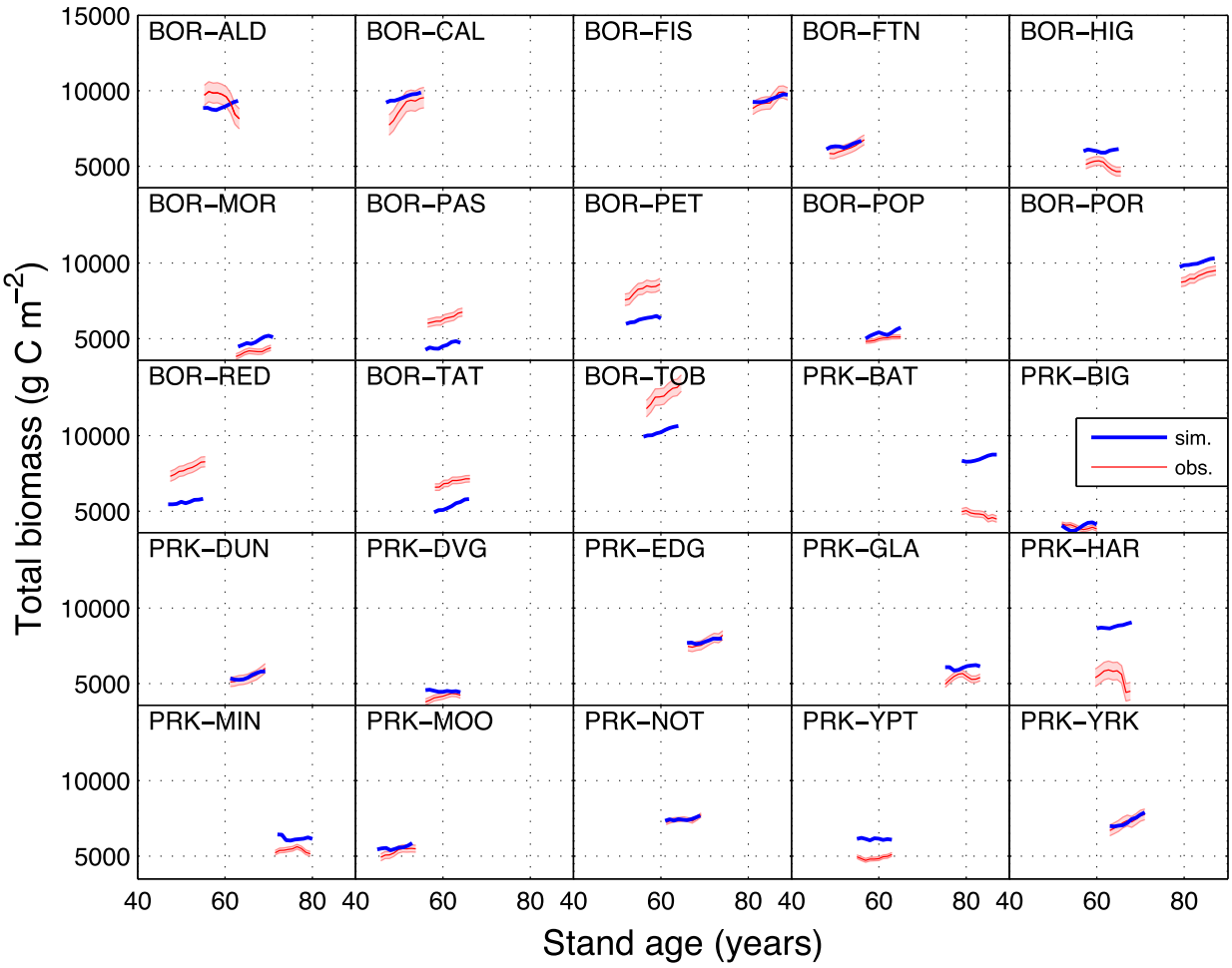

Fig. 5. Comparisons of observed and simulated total biomass at the 25 CIPHA sites during the period 2000–2008. The shaded ranges indicate error bars at one standard deviation of observed values. The first three letters (i.e., BOR and PRK) denote the site location in the boreal and parkland ecoregions, respectively. The last three letters were given by the full site names as listed in Table 1. The tree stands at PRK-BAT and PRK-HAR were affected by natural disturbance events that were not taken into account in this study (see text). Both observed and simulated data show a generally increasing biomass trend at the BOR sites and relatively little change at the PRK sites.

retention throughout the soil profile, particularly in Experiments 6S + 1C and 6L + 1C. High sensitivity to W_{soil} (steep slope) of $S_{bio,surviving}$ occurred in 3SL + 4SC, 3C + 4SC, 6C + 1S and 7C, whereas low sensitivity (gentle slope) occurred in 3S + 4SC, 6S + 1C, 6L + 1C and 7S. The simulated range of $S_{bio,surviving}$ is 4–7 times larger in the "high sensitivity" soil profiles than in the "low sensitivity" profiles. For BOR-FIS, changing the soil profile from 6L + 1C to 3SL + 4SC, produced a much greater sensitivity in $S_{bio,surviving}$ which might explain the anomalous results in Figs. 8(a) and S3. Such results indicate that soil texture assumptions can play a critical role in simulating drought-mortality relationships and should be considered carefully for future assessments of the performance of models such as Can-IBIS.

4. Discussion

4.1. Representation of water stress in Can-IBIS

The approach of using soil water constraints to simulate woody biomass mortality in Can-IBIS is based on the physical properties of soils, vertical distribution of fine roots for plant water uptake, and seasonal and interannual variations in precipitation and temperature. This approach appeared to be sufficient to describe major effects of drought stress on annual productivity of woody biomass in the boreal and prairie regions of southern Canada, but clearly some problems remain. Without a comprehensive set of detailed plant physiological experiments under drought stress conditions, soil hydrological multipliers are often used to regulate net primary productivity (e.g., Pastor and Post, 1986; Zeppel et al., 2011). Fig. 3 suggests the overall effects of water stress in contributing to woody biomass mortality were captured in Can-IBIS with some success.

Hogg et al. (2013) reported that aspen generally roots more deeply in sandy soils than in clay soils, which would clearly compensate for the lower volumetric water content generally occurring in the upper layers of a sandy profile. These researchers also found, for example, that aspen productivity was positively related to soil silt content, presumably because silty soils are able to retain more moisture than sandy soils and make more water available to plant roots at a given rooting depth. On the other hand, soils with high clay content have very low diffusivity for air and water, so tend to be poorly aerated, which restricts fine-root growth and activity. However, detailed field observations of how aspen roots develop in different soil types are lacking.

In this study, the distributions of fine-root biomass were estimated throughout the 1 m rootable soil profile based on the global analyses of Jackson et al. (1996, 1997) and used to weight water uptake from each layer. Aspen forests in the boreal region might benefit from available water in deeper soil layers if there was significant storage of water from previous years with higher than normal precipitation. Bernier et al. (2006) and Hogg et al. (2013) indicated that the aspen stands at the BOR-FIS site can draw considerable amounts water from depths greater than 1 m. Trees in

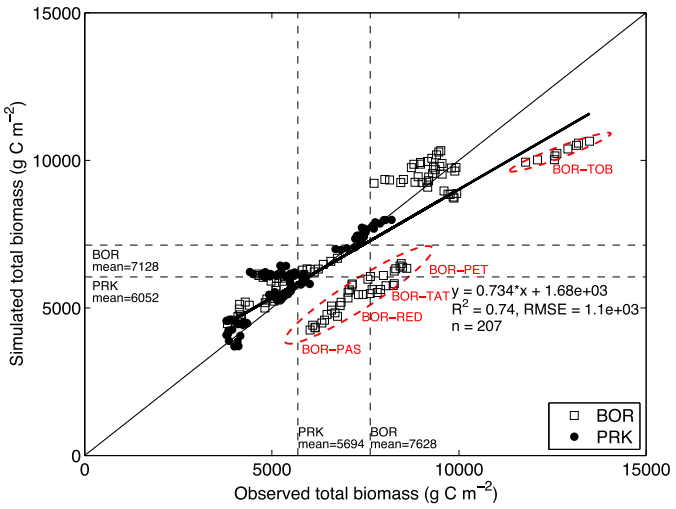

Fig. 6. Regression analysis for observed and simulated total biomass in 2000–2008. Vertical and horizontal thin dashed lines represent the means of all annual observations (*x*-axis) and all annual simulations (*y*-axis) for each of the boreal and parkland ecoregions. The diagonal thin solid line and the thick solid line are the 1:1 and fitted linear regression equation, respectively. Two ellipses circumscribing data, based on 2 standard deviations, 95% of population, show the major clusters that do not fit on the 1:1 line. Cluster no. 1: BOR-TOB; Cluster no. 2: BOR-PET, BOR-TAT, BOR-RED, and BOR-PAS. Can-IBIS is able to explain about 74% of the variation in observed biomass for all years. With the exception of these five sites in the two clusters the model predicts annual biomass in fairly close agreement with observations.

the PRK region are more vulnerable to drought due to lower mean annual precipitation and higher mean summer temperatures. The drought of 2002 through 2005 in this region was similar in intensity to the most severe drought periods of the 20th century. Both measurements and simulations showed an extremely low mean volumetric water content in the top 1 m of the soil profile during this period—falling to ~0.2 $m^3\,m^{-3}$ in 2002 compared with ~0.3 $m^3\,m^{-3}$ in 2006 (Fig. 4(a)). For the modeled assumption of an 8 m profile (Fig. 4(b)), the model was also able to simulate the changes in soil hydrological conditions during the transitions of dry and wet periods. Transitions from wet to dry periods caused reductions in LE and GPP, and conversely transitions from dry to wet caused increases in LE and GPP (Fig. 4(c) and (d)).

4.2. Drought-induced reductions in woody biomass production

The model was validated based on site-level measurements of CO_2 fluxes obtained from Fluxnet-Canada, and was able to explain approximately 90% of the observed variance (R^2 = 0.91; Fig. 4(d)) at BOR-FIS. The validated model was then applied to the 25 CIPHA study sites and found able to account for approximately 74% of the variance in observed woody biomass. In general, the interannual dynamics of GPP and total biomass (Fig. 5) were simulated reasonably well, in terms both of capturing low carbon assimilation during drought years and the overall multi-year trends in biomass growth. Because of the generally drier climate in the PRK region, observed and simulated woody biomass growth were slower in PRK than in BOR. The model was also able to discriminate the observed differences in mean biomass between the two regions quite accurately (the BOR region having approximately 1900 g C m^{-2} more standing biomass than the PRK region).

The model suggested that total biomass was reduced by 5–7% (100 to 400 g C m^{-2}) at the PRK-EDG and PRK-NOT sites during 2002. Both observations and simulations showed decreased biomass growth or no significant increase in biomass at five representative CIPHA sites (see Supplementary information, Fig. S3) with the model able to capture the overall differences among sites. Some stochastic variation may occur in the observations at CIPHA sites, given that mortality is a patchy phenomenon and monitoring was limited to three stands per site. Our results confirm that aspen stands in the parkland region of southern Alberta and Saskatchewan are at greater risk of die-back due to the generally drier environment than that of aspen stands in the mixed woods of the boreal forest further north.

Assessment of drought intensity is often based on calculations of drought indices (Hogg et al., 2005; Sheffield et al., 2012) for characterizing and monitoring drought conditions at large spatial and temporal scales. In this study, the self-calibrated Palmer Drought Severity Index, $PDSI_{sc}$ was adopted as a "relative" index to investigate differences in drought intensity across the study region and to examine its relationship with surviving biomass. Although $PDSI_{sc}$ reports whether short-term conditions are relatively wetter

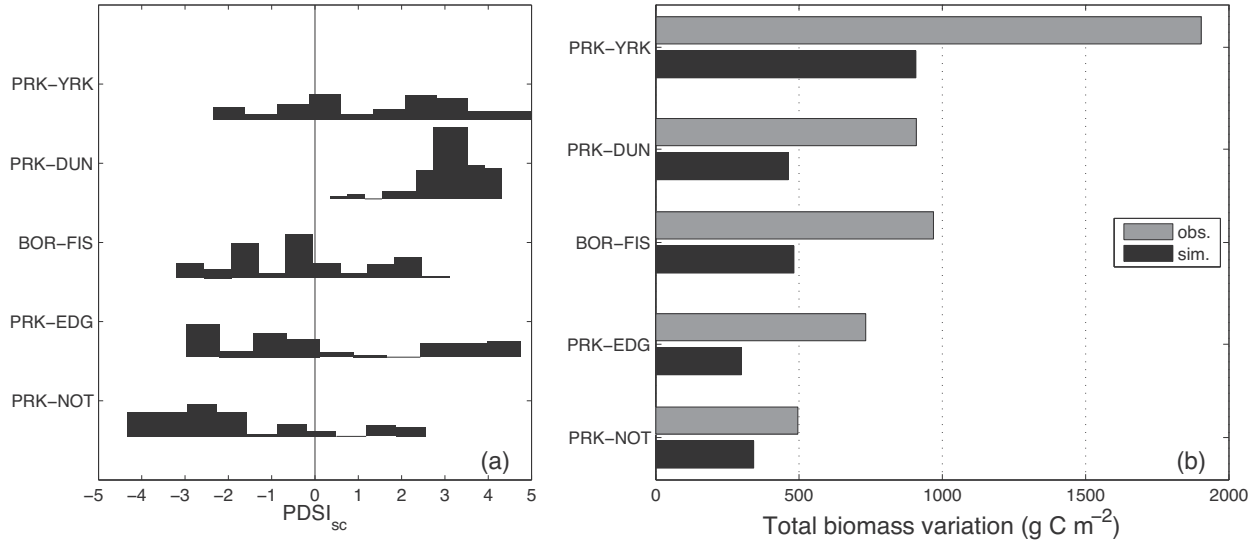

Fig. 7. Observed and simulated biomass variation response to $PDSI_{sc}$ at five selected study sites in the CIPHA network from 2000 to 2008. (a) Histograms of accumulated distributions of monthly PDSIsc classes; the distribution indicates the frequency (in months) of occurrence of each $PDSI_{sc}$ class over 108 months (9 years); (b) accumulated biomass changes in each year, presenting the variation between annual totals in the study period. The overall tendency of biomass variation corresponded to the drought signals inferred from the regional $PDSI_{sc}$.

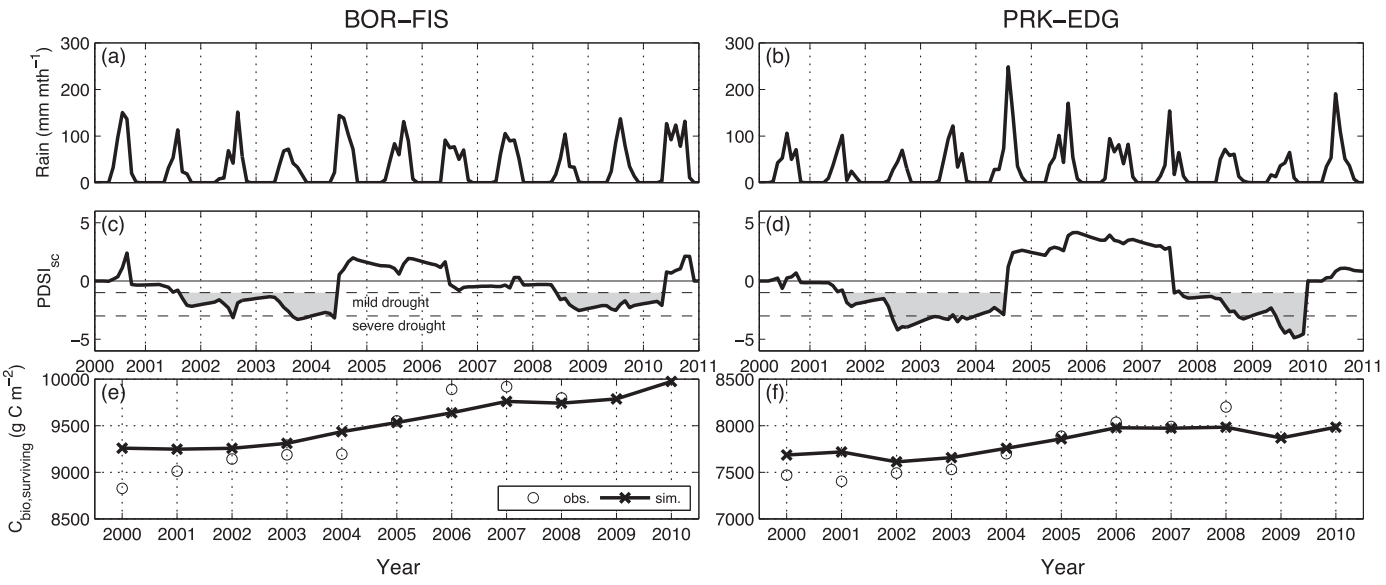

Fig. 8. Surviving biomass responses to monthly accumulated rain and self-calibrated PDSI at two CIPHA study sites: (a)–(c)–(e) BOR-FIS and (b)–(d)–(f) PRK-EDG. The shaded areas indicate where $PDSI_{sc}$ reaches a significant drought condition ($PDSI_{sc} < -1.0$). Can-IBIS simulates increased biomass mortality in response to the more intense droughts indicated by lower rainfall and the shaded areas of $PDSI_{sc}$ in 2001–2003 and 2008–2009.

or drier than the long-term average for a given site, this index was also generally correlated with the observed variations in woody biomass accumulation at most CIPHA sites (Fig. 7). Smaller total biomass variations were observed at sites where more negative $PDSI_{sc}$ (i.e., generally drier conditions) occurred, particularly PRK-EDG and PRK-NOT.

4.3. Uncertainties and implications: Forest die-back and vegetation shift in a changing climate

In this study, monthly climate data interpolated to 10 km spatial resolution were used to force the internal Richardson WGEN weather generator to simulate hourly weather data which were then applied at the site level. Therefore, a fundamental uncertainty exists in the accuracy of the forcing meteorology used at each CIPHA site. The overall pattern of daily precipitation was captured fairly poorly (Fig. S1). For example, overestimated precipitation during the summer of 2002 (Fig. S2) would have increased W_{soil} in the top 1 m soil depth (Fig. 4) for a period. We have assumed that annual mortality is a function of the cumulative water stress during the growing season. The model calculates these values at hourly timesteps and clearly these are subject to variations at daily time scales. Because the modeled responses of plant growth and allocation to woody biomass to variations in soil water are highly non-linear, it is logical to use these daily variations as the forcing. Furthermore, the very poor spatial resolution of soil texture and related physical properties is likely to create a mismatch between model results and observed data, which could create significant discrepancies in simulated biomass growth and mortality (Fig. 9(b)). Soil texture in deep soil layers may be particularly important because texture represents a major control on water accumulation and drainage throughout the soil column.

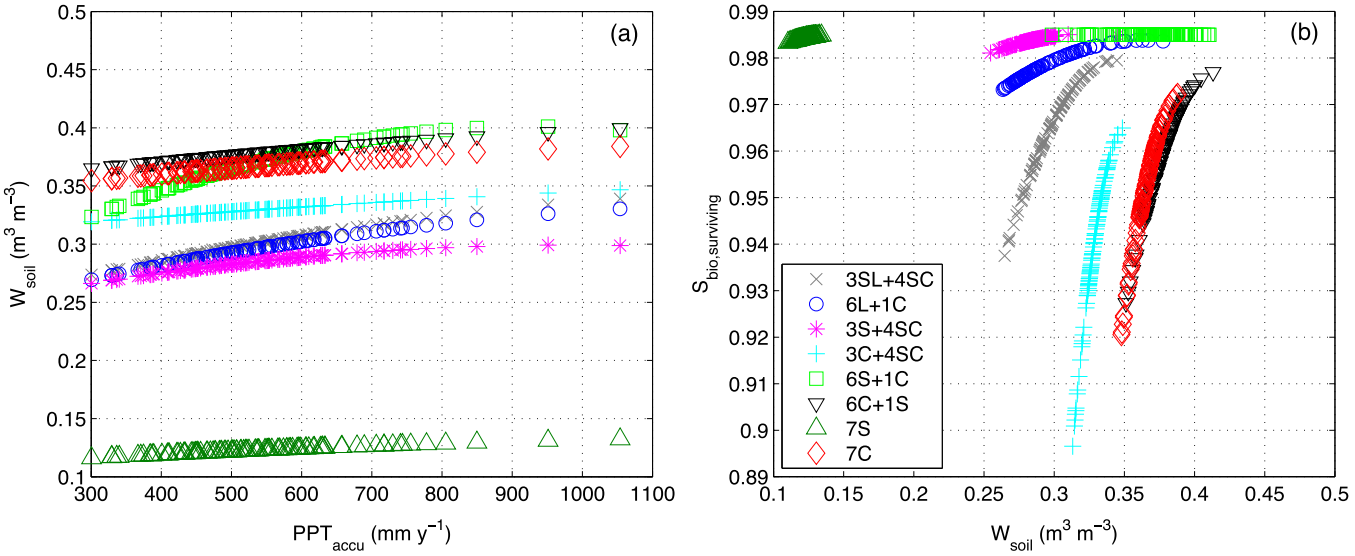

Fig. 9. Results from sensitivity experiments to explore effects of different soil texture profiles on relationships between (a) annual precipitation and volumetric water content in the total 8 m soil column; and (b) volumetric water content and surviving biomass. The codes for each soil texture profile are provided in Table 2. Results indicate that soil texture assumptions can play a critical role in simulating drought-mortality relationships.

Landhäusser and Lieffers (2011) pointed out that drought effects during the growing season can play an important role in the decline and mortality of mature trees. In this study, water stress was accumulated throughout the growing season to create a biomass mortality factor (i.e., Eq. (4)). Further complexities include changes in the capacity of drought-stressed plants to mobilize stored carbohydrates (to alter osmotic potential, e.g., to avoid irreversible damage to metabolic pathways), and the refilling of embolized xylem following severe drought conditions. Drought may also increase susceptibility of forest vegetation to disease and insect attacks or wildfire. Hence, simulating drought effects on biomass production and mortality requires a more integrated approach that accounts for the interaction of plant physiological mechanisms, hydrological effects and exogenous disturbance factors. The mechanisms of biomass mortality are complex and uncertain and differ among tree species, potentially involving human activities as well as biotic factors (e.g., Martinez-Vilalta et al., 2012; Zeppel et al., 2011).

An underlying objective of this work is to be able to use Can-IBIS to investigate effects of climate change on vegetation composition and carbon cycles. Drought-induced biomass mortality may be enhanced by combinations of other ecological factors, including insect outbreaks (Worrall et al., 2008, 2010), and wildfire occurrence (Davies et al., 2010). Ultimately, mortality enhances changes in vegetation composition (Amiro et al., 2006; Chiatante et al., 2006; Hebert et al., 2006; Huddle and Pallardy, 1996; Spies et al., 2006). Forest die-back (abnormally rapid senescence of branches and twigs) is likely to increase in future as plant communities are increasingly exposed to multiple climatically induced stresses with more frequent and/or intense extremes. This will in turn lead to greater landscape-level responses to climatic variation, and ultimately changes in the presence and/or composition of forest vegetation can be expected (Allen et al., 2010; Hogg et al., 2005; Michaelian et al., 2010). In the transition ecozone (i.e., the PRK region) in the southern boreal forests of western Canada, young trees and vegetation succession may be influenced by more frequent future droughts, altering terrestrial carbon stocks. The ultimate goal of this study was to use available coarse resolution data (as would be used for prognostic simulations) with a single set of parameters applied at all sites. On balance, our results indicate process-based models (such as DVMs) can be used to simulate changes in regional properties of vegetation, and hence contribute to improvements in understanding of the global carbon budget and vegetation-climate feedbacks (e.g., Quillet et al., 2010).

5. Conclusions

A modified version of the Integrated Blosphere Simulator applied to Canadian forest ecosystems (Can-IBIS) was quite successful in reproducing measured monthly latent heat flux and gross primary productivity over several years using only monthly climate data interpolated to coarse spatial resolution (~10 km). A significant problem occurred in the simulation of seasonal and interannual variations in soil moisture content, however, which was attributed, at least partially, to low quality soils data. A modeling experiment using eight alternative representations of the soil texture profile at the forest site indicated high sensitivity of modeled soil moisture content and drought stress to the parameterization of soil texture and its vertical distribution in the soil profile. A correct parameterization of the soil profile appears to be critically important when simulating changes in the site water balance and its impacts on forest productivity and biomass accumulation.

With these limitations on the representation of soil moisture dynamics in mind, the model was used to simulate effects of soil water stress, including multi-year drought events, on growth and mortality of woody biomass (predominantly trembling aspen) at 25 sites in the Climate Impacts on Productivity and Health of Aspen (CIPHA) network of Hogg et al. (2005). The model was able to explain approximately 74% of the variance in woody biomass growth observed over the period 2000 to 2008 (nine years) at the 25 sites. Simulated mortality of biomass corresponded to observed temporal and spatial variations in drought intensity, reaching 5–7% (100 to 400 g C m^{-2}) during 2002, considered to be driest year of the nine-year period (and one of the driest on record). The model also estimated lower biomass mortality in the boreal region than the drier parkland region, indicating a realistic response to higher mean annual precipitation. However, the model's capacity to predict short term variations in biomass growth was limited by the lack of spatially accurate data on soil physical properties, by poor internal generation of weather data at hourly and daily time scales, and to some extent by the simplifications of plant ecophysiological responses to drought effects. More specific physiological information will be required to further refine the model's simulation of biomass mortality for other plant functional types.

Acknowledgements

This research was supported by a Strategic Grant Project (STPGP 381474-09) of the Natural Science and Engineering Council of Canada (NSERC). We thank Tim Boland helped with the model calibration, input data and simulation scripts in cluster computers. Dr. Jinxun Liu and Jean-Sébastien Landry provided the earlier version of Can-IBIS source code and insights for parameterization. Nathan Wells and Dr. Steve Goddard provided the PDSI source code. Dr. Jonathan Dursi helped with evaluation of model stability across different computing platforms in SciNet, Compute/Calcul Canada. Stephen Kull provided the suggestions with source code of CBM-CFS3 and modeling strategies. Michael Michaelian provided the sampling protocols and maps for CIPHA. We also thank Drs. Andrew Black, Lawrence Flanagan, Paul Bartlet, Ralf Staebler, Altaf Arain, Brian Amiro and Hank Margolis to provide the flux tower measurements. Helpful comments on the earlier version of manuscript were provided by two anonymous reviewers.

Appendix A. Supplementary data

Supplementary data associated with this article can be found, in the online version, at http://dx.doi.org/10.1016/j.agrformet.2014.07.013.

References

Adams, H.D., Guardiola-Claramonte, M., Barron-Gafford, G.A., Villegas, J.C., Breshears, D.D., Zou, C.B., Troch, P.A., Huxman, T.E., 2009. Temperature sensitivity of drought-induced tree mortality portends increased regional die-off under global-change-type drought. Proc. Nat. Acad. Sci. U.S.A. 106, 7063–7066.

Allen, C.D., Macalady, A.K., Chenchouni, H., Bachelet, D., McDowell, N., Vennetier, M., Kitzberger, T., Rigling, A., Breshears, D.D., Hogg, E.H., Gonzalez, P., Fensham, R., Zhang, Z., Castro, J., Demidova, N., Lim, J.H., Allard, G., Running, S.W., Semerci, A., Cobb, N., 2010. A global overview of drought and heat-induced tree mortality reveals emerging climate change risks for forests. Forest Ecol., Manage. 259, 660–684.

Amiro, B.D., Barr, A.G., Black, T.A., Iwashita, H., Kljun, N., McCaughey, J.H., Morgenstern, K., Murayama, S., Nesic, Z., Orchansky, A.L., Saigusa, N., 2006. Carbon, energy and water fluxes at mature and disturbed forest sites, Saskatchewan, Canada. Agric. For. Meteorol. 136, 237–251.

Ball, J.T., Woodrow, I.E., Berry, J.A., 1987. A model predicting stomatal conductance and its contribution to the control of photosynthesis under different environmental conditions. Progr. Photosynth. Res. 4, 221–224.

Barr, A.G., Black, T.A., Hogg, E.H., Griffis, T.J., Morgenstern, K., Kljun, N., Theede, A., Nesic, Z., 2007. Climatic controls on the carbon and water balances of a boreal aspen forest, 1994–2003. Global Change Biol. 13, 561–576.

Bernier, P.Y., Bartlett, P., Black, T.A., Barr, A., Kljun, N., McCaughey, J.H., 2006. Drought constraints on transpiration and canopy conductance in mature aspen and jack pine stands. Agric. For. Meteorol. 140 (1–4), 64–78.

Bonan, G.B., 1994. Comparison of 2 land-surface process models using prescribed forcings. J. Geophys. Res. D: Atmos. 99, 25803–25818.
Brandt, J.P., Flannigan, M.D., Maynard, D.G., Thompson, I.D., Volney, W.J.A., 2013. An introduction to Canada's boreal zone: ecosystem processes, health, sustainability, and environmental issues. Environ. Rev. 21, 207–226.
Chiatante, D., Di Iorio, A., Sciandra, S., Scippa, G.S., Mazzoleni, S., 2006. Effect of drought and fire on root development in *Quercus pubescens* Willd. and *Fraxinus ornus* L. seedlings. Environ. Exp. Bot. 56, 190–197.
Cuenca, R.H., Stangel, D.E., Kelly, S.F., 1997. Soil water balance in a boreal forest. J. Geophys. Res. D: Atmos. 102, 29355–29365.
Davies, G.M., Legg, C.J., O'Hara, R., MacDonald, A.J., Smith, A.A., 2010. Winter desiccation and rapid changes in the live fuel moisture content of *Calluna vulgaris*. Plant Ecol. Diversity 3, 289–299.
Delbart, N., Ciais, P., Chave, J., Viovy, N., Malhi, Y., Le Toan, T., 2010. Mortality as a key driver of the spatial distribution of above-ground biomass in Amazonian forest: results from a dynamic vegetation model. Biogeosciences 7, 3027–3039.
Di Iorio, A., Montagnoli, A., Scippa, G.S., Chiatante, D., 2011. Fine root growth of *Quercus pubescens* seedlings after drought stress and fire disturbance. Environ. Exp. Bot. 74, 272–279.
El Maayar, M., Price, D.T., Black, T.A., Humphreys, E.R., Jork, E.M., 2002. Sensitivity tests of the integrated biosphere simulator to soil and vegetation characteristics in a Pacific coastal coniferous forest. Atmosphere—Ocean 40, 313–332.
El Maayar, M., Price, D.T., Chen, J.M., 2009. Simulating daily, monthly and annual water balances in a land surface model using alternative root water uptake schemes. Adv. Water Resour. 32, 1444–1459.
Farquhar, G.D., Caemmerer, S., Berry, J.A., 1980. A biochemical model of photosynthetic CO_2 assimilation in leaves of C3 species. Planta 149, 78–90.
Flanagan, L.B., Johnson, B.G., 2005. Interacting effects of temperature, soil moisture and plant biomass production on ecosystem respiration in a northern temperate grassland. Agric. For. Meteorol. 130, 237–253.
Foley, J.A., Prentice, I.C., Ramankutty, N., Levis, S., Pollard, D., Sitch, S., Haxeltine, A., 1996. An integrated biosphere model of land surface processes, terrestrial carbon balance, and vegetation dynamics. Global Biogeochem. Cycles 10, 603–628.
Garcia-Quijano, J.F., Barros, A.P., 2005. Incorporating canopy physiology into a hydrological model: photosynthesis, dynamic respiration, and stomatal sensitivity. Ecol. Model. 185, 29–49.
Granier, A., Reichstein, M., Bréda, N., Janssens, I.A., Falge, E., Ciais, P., Gruenwald, T., Aubinet, M., Berbigier, P., Bernhofer, C., Buchmann, N., Facini, O., Grassi, G., Heinesch, B., Ilvesniemi, H., Keronen, P., Knohl, A., Koestner, B., Lagergren, F., Lindroth, A., Longdoz, B., Loustau, D., Mateus, J., Montagnani, L., Nys, C., Moors, E., Papale, D., Peiffer, M., Pilegaard, K., Pita, G., Pumpanen, J., Rambal, S., Rebmann, C., Rodrigues, A., Seufert, G., Tenhunen, J., Vesala, I., Wang, Q., 2007. Evidence for soil water control on carbon and water dynamics in European forests during the extremely dry year: 2003. Agric. For. Meteorol. 143, 123–145.
Hebert, F., Boucher, J.F., Bernier, P.Y., Lord, D., 2006. Growth response and water relations of 3-year-old planted black spruce and jack pine seedlings in site-prepared lichen woodlands. Forest Ecol. Manage. 223, 226–236.
Hogg, E.H., Barr, A.G., Black, T.A., 2013. A simple soil moisture index for representing multi-year drought impacts on aspen productivity in the western Canadian interior. Agric. For. Meteorol. 178–179, 173–182.
Hogg, E.H., Brandt, J.P., Kochtubajda, B., 2005. Factors affecting interannual variation in growth of western Canadian aspen forests during 1951–2000. Can. J. For. Res. 35, 610–622.
Huddle, J.A., Pallardy, S.G., 1996. Effects of soil and stem base heating on survival, resprouting and gas exchange of *Acer* and *Quercus* seedlings. Tree Physiol. 16, 583–589.
Hutchinson, M.F., 2004. ANUSPLIN Version 4.3. Centre for Resource and Environmental Studies, The Australian National University, Canberra, Australia.
IPCC, 2007. Climate change 2007: the physical science basis. In: Solomon, S.D. (Ed.), Contribution of Working Group I to the Fourth Assessment Report of the Intergovernmental Panel on Climate Change. Cambridge University Press, Cambridge, United Kingdom.
Jackson, R.B., Canadell, J., Ehleringer, J.R., Mooney, H.A., Sala, O.E., Schulze, E.D., 1996. A global analysis of root distributions for terrestrial biomes. Oecologia 108, 389–411.
Jackson, R.B., Mooney, H.A., Schulze, E.D., 1997. A global budget for fine root biomass, surface area, and nutrient contents. Proc. Nat. Acad. Sci. U.S.A. 94, 7362–7366.
Kreyling, J., Wenigmann, M., Beierkuhnlein, C., Jentsch, A., 2008. Effects of extreme weather events on plant productivity and tissue die-back are modified by community composition. Ecosystems 11, 752–763.
Kucharik, C.J., Foley, J.A., Delire, C., Fisher, V.A., Coe, M.T., Lenters, J.D., Young-Molling, C., Ramankutty, N., Norman, J.M., Gower, S.T., 2000. Testing the performance of a dynamic global ecosystem model: water balance, carbon balance, and vegetation structure. Global Biogeochem. Cycles 14, 795–825.
Lambert, M.C., Ung, C.H., Raulier, F., 2005. Canadian national tree aboveground biomass equations. Can. J. For. Res. 35, 1996–2018.
Landhäusser, S.M., Lieffers, V.J., 2011. Defoliation increases risk of carbon starvation in root systems of mature aspen. Trees 26, 653–661.
Liu, J.X., Price, D.T., Chen, J.M., 2005. Nitrogen controls on ecosystem carbon sequestration: a model implementation and application to Saskatchewan, Canada. Ecol. Model. 186, 178–195.
Ma, Z., Peng, C., Zhu, Q., Chen, H., Yu, G., Li, W., Zhou, X., Wang, W., Zhang, W., 2012. Regional drought-induced reduction in the biomass carbon sink of Canada's boreal forests. Proc. Nat. Acad. Sci. U.S.A. 109, 2423–2427.
Martinez-Vilalta, J., Lloret, F., Breshears, D., 2012. Drought-induced forest decline: causes, scope and implications. Biol. Lett. 8, 689–691.
McKenney, D.W., Pedlar, J.H., Papadopol, P., Hutchinson, M.F., 2006. The development of 1901–2000 historical monthly climate models for Canada and the United States. Agric. For. Meteorol. 138, 69–81.
McKenney, D.W., Pedlar, J.H., Rood, R.B., Price, D.T., 2011. Revisiting projected shifts in the climate envelopes of North American trees using updated general circulation models. Global Change Biol. 7, 2720–2730.
Michaelian, M., Hogg, E.H., Hall, R.J., Arsenault, E., 2010. Massive mortality of aspen following severe drought along the southern edge of the Canadian boreal forest. Global Change Biol. 17, 2084–2094.
Parton, W.J., Scurlock, J.M.O., Ojima, D.S., Gilmanov, T.G., Scholes, R.J., Schimel, D.S., Kirchner, T., Menaut, J.C., Seastedt, T., Moya, E.G., Kamnalrut, A., Kinyanario, J.I., 1993. Observations and modeling of biomass and soil organic matter dynamics for the grassland biome worldwide. Global Biogeochem. Cycles 7, 785–809.
Pastor, J., Post, W.M., 1986. Influence of climate, soil moisture, and succession on forest carbon and nitrogen cycles. Biogeochemistry 2 (1), 3–27.
Peng, C., Ma, Z., Lei, X., Zhu, Q., Chen, H., Wang, W., Liu, S., Li, W., Fang, X., Zhou, X., 2011. A drought-induced pervasive increase in tree mortality across Canada's boreal forests. Nat. Clim. Change 1, 467–471.
Quillet, A., Peng, C., Garneau, M., 2010. Toward dynamic global vegetation models for simulating vegetation-climate interactions and feedbacks: recent developments, limitations, and future challenges. Environ. Rev. 18, 333–353.
Richardson, C.W., Wright, D.A., 1984. WGEN: a model for generating daily weather variables. In: ARS-8 88. US Department of Agriculture, Agricultural Research Service.
Sala, A., 2009. Lack of direct evidence for the carbon-starvation hypothesis to explain drought-induced mortality in trees. Proc. Nat. Acad. Sci. U.S.A. 106, E68.
Schwalm, C.R., Williams, C.A., Schaefer, K., Baldocchi, D., Black, T.A., Goldstein, A.H., Law, B.E., Oechel, W.C., Kyaw, T.P.U., Scott, R.L., 2012. Reduction in carbon uptake during turn of the century drought in western North America. Nat. Geosci. 5 (8), 551–556.
Sheffield, J., Wood, E.F., Roderick, M.L., 2012. Little change in global drought over the past 60 years. Nature 491, 435–438.
Soil Landscapes of Canada Working Group, 2004. Soil Landscapes of Canada Version 3.0. Agriculture and Agri-Food Canada.
Spies, T.A., Hemstrom, M.A., Youngblood, A., Hummel, S., 2006. Conserving old-growth forest diversity in disturbance-prone landscapes. Conserv. Biol. 20, 351–362.
Tague, C.L., McDowell, N.G., Allen, C.D., 2013. An integrated model of environmental effects on growth, carbohydrate balance, and mortality of *Pinus ponderosa* forests in the Southern Rocky Mountains. PLoS One 8 (11).
Thompson, S.L., Pollard, D., 1995a. A global climate model (GENE-SIS) with a land-surface transfer scheme (LSX). Part I. Present climate simulation. J. Clim. 8, 732–761.
Thompson, S.L., Pollard, D., 1995b. A global climate model (GEN-ESIS) with a land-surface transfer scheme (LSX). Part II. CO_2 sensitivity. J. Clim. 8, 1104–1121.
van der Molen, M.K., Dolman, A.J., Ciais, P., Eglin, T., Gobron, N., Law, B.E., Meir, P., Peters, W., Phillips, O.L., Reichstein, M., Chen, T., Dekker, S.C., Doubková, M., Friedl, M.A., Jung, M., van den Hurk, B.J.J.M., de Jeu, R.A.M., Kruijt, B., Ohta, T., Rebel, K.T., Plummer, S., Seneviratne, S.I., Sitch, S., Teuling, A.J., van der Werf, G.R., Wang, G., 2011. Drought and ecosystem carbon cycling. Agric. For. Meteorol. 151, 765–773.
Verberne, E.L.J., Hassink, J., Dewilligen, P., Groot, J.J.R., Vanveen, J.A., 1990. Modeling organic-matter dynamics in different soils. Neth. J. Agric. Sci. 38, 221–238.
Wang, W., Peng, C., Kneeshaw, D.D., Larocque, G.R., Luo, Z., 2012. Drought-induced tree mortality: ecological consequences, causes, and modeling. Environ. Rev. 20, 109–121.
Wang, X., Fang, J., Zhu, B., 2008. Forest biomass and root-shoot allocation in northeast China. Forest Ecol. Manage. 255, 4007–4020.
Wells, N., Goddard, S., Hayes, M.J., 2004. A self-calibrating Palmer Drought Severity Index. J. Clim. 17, 2335–2351.
Worrall, J.J., Egeland, L., Eager, T., Mask, R.A., Johnson, E.W., Kemp, P.A., Shepperd, W.D., 2008. Rapid mortality of *Populus tremuloides* in southwestern Colorado, USA. Forest Ecol. Manage. 255, 686–696.
Worrall, J.J., Marchetti, S.B., Egeland, L., Mask, R.A., Eager, T., Howell, B., 2010. Effects and etiology of sudden aspen decline in southwestern Colorado, USA. Forest Ecol. Manage. 260, 638–648.
Zeppel, M.J.B., Adams, H.D., Anderegg, W.R.L., 2011. Mechanistic causes of tree drought mortality: recent results, unresolved questions and future research needs. New Phytol. 192, 800–803.
Zhao, M.S., Running, S.W., 2010. Drought-induced reduction in global terrestrial net primary production from 2000 through 2009. Science 329, 940–943.
Zheng, Z., Wang, G., 2007. Modeling the dynamic root water uptake and its hydrological impact at the Reserva Jaru site in Amazonia. J. Geophys. Res. G: Biogeosci. 112, G04012.